Processing the Blackfoot 3C-3D seismic survey

Vladan Simin, Mark P. Harrison and Gary A. Lorentz

ABSTRACT

In November 1995, a 3C-3D survey was acquired over the Blackfoot field located near Strathmore, Alberta, Canada (T23 R23 W5M). Processing was performed by Pulsonic Geophysical and Sensor Geophysical, two of the most experienced contractors in 3C processing.

The three components were separated out and processed to deconvolution. At this point two horizontal components were rotated and birefringence analysis was performed, while vertical channel data were processed using the conventional P-wave processing flow. Both radial and transverse data volumes were processed through to post-stack time migration using asymptotic, depth-variant and DMO binning.

INTRODUCTION

This report describes the processing of a seismic data set recorded for the Blackfoot consortium, under the supervision of Boyd Petrosearch. The 6.5 square mile survey was consists of two distinct sections - high fold patch, targeting Glauconitic channel sands of Lower Mannville and long offset patch targeting deeper Swan Hills reef-prone carbonates (as shown in figure 1.).

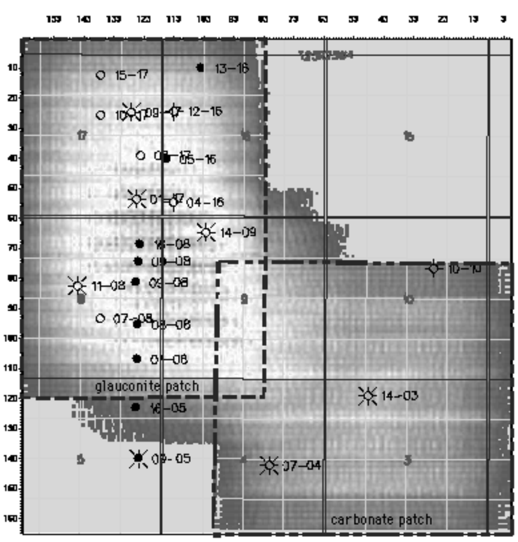

Fig.1. Fold map of the Blackfoot 3C 3D seismic survey

Full data set was sent to Pulsonic on November 22,1995, while Sensor processed the high fold portion of the survey in the March to May 1996 time frame. Figures 1 is a fold map of the survey showing high fold portion processed by Sensor and long offsets, carbonate patch. The following will describe in detail the processing sequence of these data sets.

DATA ANALYSIS

This is a three component dataset, therefore the shot records had to be separated into vertical, north(H1) and east(H2) components before processing could begin. Figure 2 shows portion of the separated components record for FFID 201.

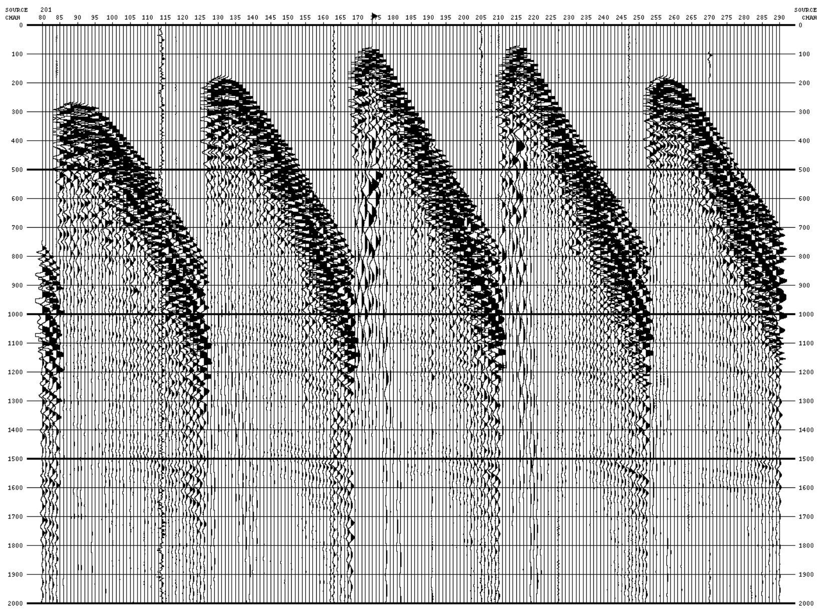

a)

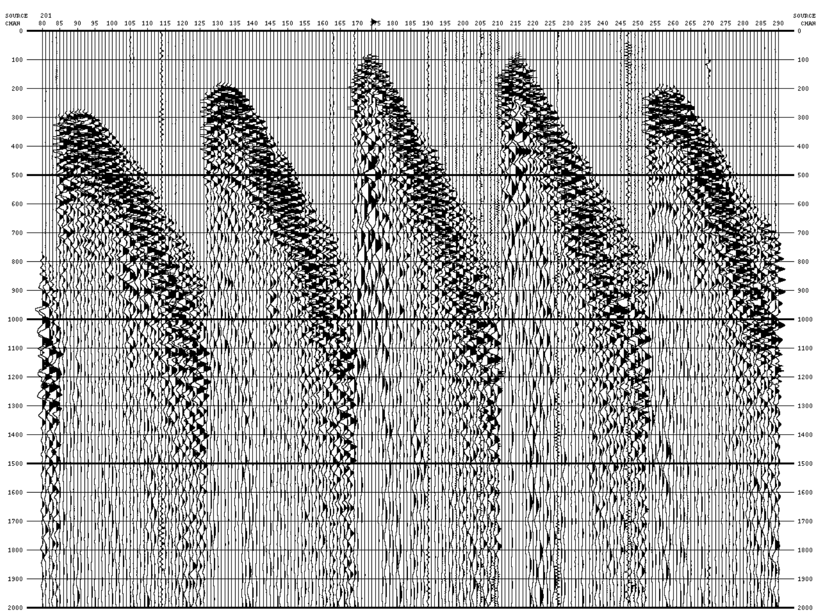

b)

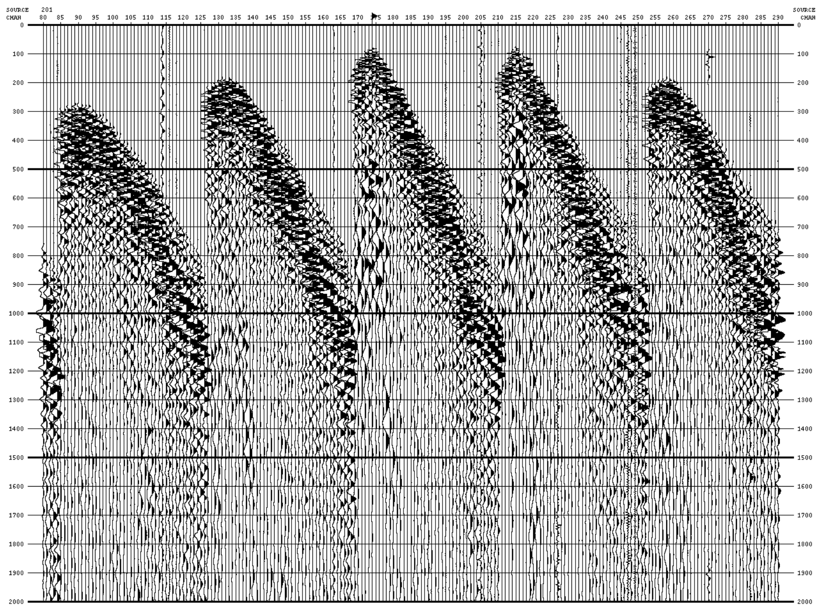

c)

Fig.2. Portion of representative field records from a) vertical, b) north and c) east components

After component separation, data was analyzed for birefringence effects. The method involved processing the two horizontal components up to the deconvolution stage, then rotating to radial and transverse directions for each shot-receiver pair and stacking data into limited azimuth receiver stacks. Data were stacked in 30 degree azimuth increments, with a 30 degree aperture. This provided a reasonable signal to noise ratio on the stacks, which could then be interpreted to determine the effects of shear wave splitting on this dataset.

After the analysis, the radial component was found to contain signal energy at all azimuths, while the transverse component showed very little signal energy at all azimuths. This led to a conclusion that there was no significant shear wave splitting present. As a result, data was fully processed to radial stacked section only. A transverse stacked section was produced for completeness using parameters derived from the radial volume.

PROCESSING FLOWS

The raw records were input from a demultiplexed SEG-D format. The 2070 channel shot records were separated into three data sets of 690 channel records.

Initial testing on the data included a filter and deconvolution tests performed on several vertical and horizontal raw records. Frequency tests showed the bandwidth to be between 5 and 90 Hz for the vertical data and 5 to 50 Hz for the horizontal data although preserved bandwidth on the final stacked volumes has narrowed to 10-80 Hz and 8-45 Hz respectively. Initial bandwidth information was used in determining the output spectrum for deconvolution as well as display filters for quality control product.

Decon tests were performed with signature and spiking deconvolution methods using variable operator lengths and pre-whitening parameters. The four-component surface consistent designature was chosen on the basis of its ability to produce sharp, continuous reflections at shallow depths, relatively clean autocorrelation and flat output spectrum. Using this method, ensemble-averaged log-amplitude spectra for the shot, receiver, offset and CDP components are subtracted from the average log-amplitude spectrum for the entire data set. Residuals for the shot and receiver components were used for computation of the deconvolution operator because these components represent near surface effects. Pulsonic's processing flows for the vertical and radial component data are outlined in figures 3 and 4.

SEG-D REFORMATTED DEMULTIPLEX INPUT
COMPONENT SEPARATION
3D GEOMETRY ASSIGNMENT
TRACE EDITS

SURFACE CONSISTENT AMPLITUDE BALANCE
SURFACE CONSISTENT DECONVOLUTION

HORIZONTAL COMPONENT ROTATION
ELEVATION AND REFRACTION STATICS
RESIDUAL SURFACE CONSISTENT STATICS

ASYMPTOTIC CCP MACROBIN SORT
VELOCITY ANALYSIS
3D NMO CORRECTION

VELOCITY SPECIFIC FILTER
FK MEDIAN FILTER
TRACE MUTE

3D CONVERTED WAVE DMO
3D CCP BIN STACK

F/X MIGRATION
SPECTRAL BALANCE
FXY DECONVOLUTION
BANDPASS FILTER
TIME VARIANT SCALING

Fig.3. Pulsonic's vertical processing flow

SEG-D REFORMATTED DEMULTIPLEX INPUT
COMPONENT SEPARATION
3D GEOMETRY ASSIGNMENT
TRACE EDITS

SURFACE CONSISTENT AMPLITUDE BALANCE
SURFACE CONSISTENT DECONVOLUTION

HORIZONTAL COMPONENT ROTATION
ELEVATION AND REFRACTION STATICS
RESIDUAL SURFACE CONSISTENT STATICS

ASYMPTOTIC CCP MACROBIN SORT
VELOCITY ANALYSIS
3D NMO CORRECTION

VELOCITY SPECIFIC FILTER
FK MEDIAN FILTER
TRACE MUTE

3D CONVERTED WAVE DMO
3D CCP BIN STACK
F/X MIGRATION
SPECTRAL BALANCE
FXY DECONVOLUTION
BANDPASS FILTER
TIME VARIANT SCALING

Fig.4. Pulsonic's radial processing flow

When computing the decon operator for horizontal data, the dual nature of the converted waves allows one to calculate the shot component of the decon operator from the vertical data and receiver component from the horizontal data. This was also true for the refraction statics calculations where shot statics from P-P data were added to the receiver statics from P-S data .

Velocity analysis was performed every 450m. The time-shifted hyperbola equation was used to calculate and apply the velocities for horizontal data's NMO corrections. While CMP stacking of vertical gathers is a straight-forward process, radial gathers had to be corrected for dip moveout effects before CCP bin stacking could be performed. In addition to DMO binned data Sensor also produced asymptotic only and depth variant binning stacks. Figures 5 and 6 outline Sensor’s radial and vertical processing flows.

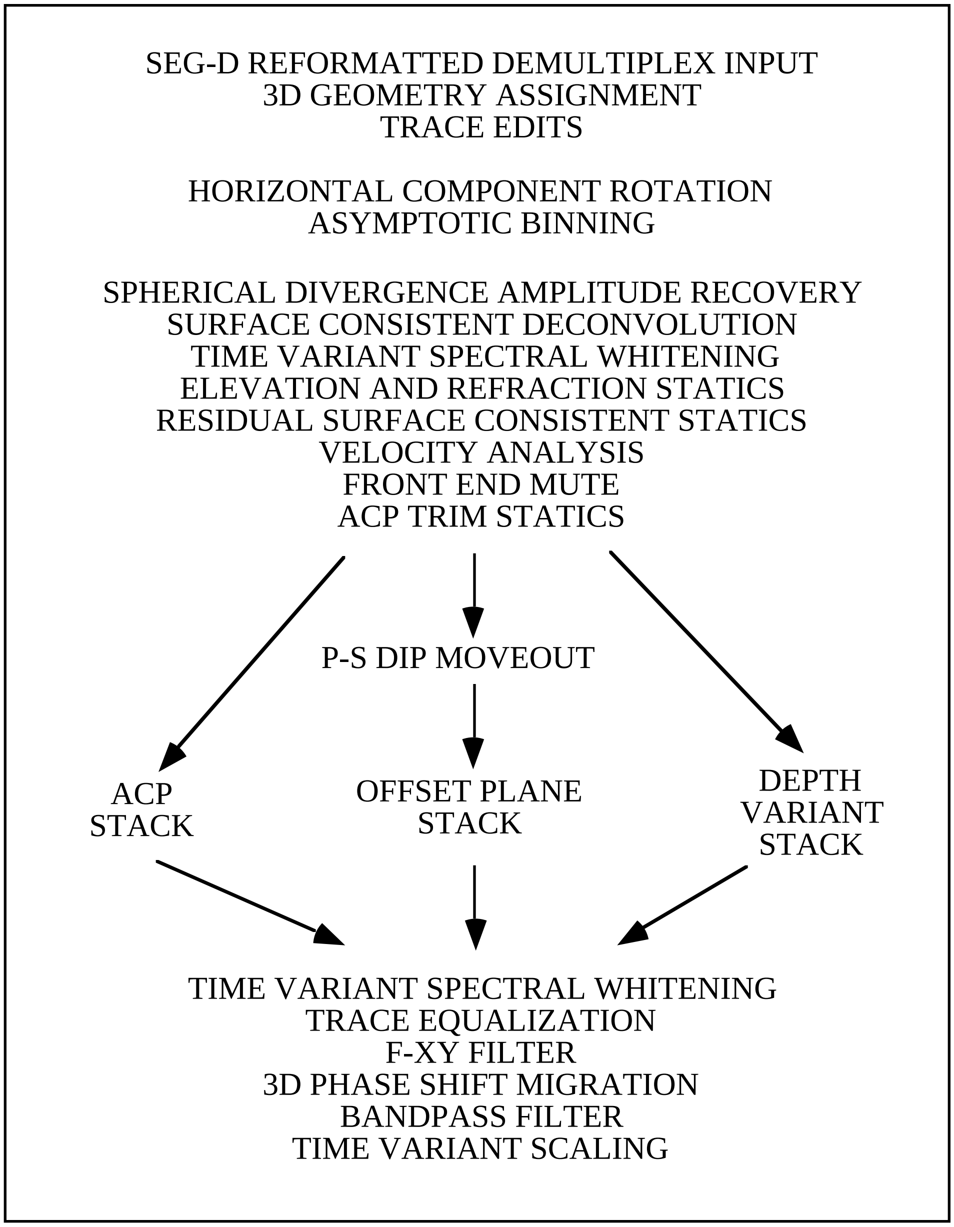

Fig.5. Sensor's radial processing flow for Asymptotic, DMO and Depth Variant binning methods

SEG-D REFORMATTED DEMULTIPLEX INPUT
3D GEOMETRY ASSIGNMENT
TRACE EDITS

SPHERICAL DIVERGENCE AMPLITUDE RECOVERY
SURFACE CONSISTENT DECONVOLUTION
TIME VARIANT SPECTRAL WHITENING
ELEVATION AND REFRACTION STATICS
RESIDUAL SURFACE CONSISTENT STATICS
VELOCITY ANALYSIS
FRONT END MUTE
TRIM STATICS
CDP STACK

TIME VARIANT SPECTRAL WHITENING
TRACE EQUALIZATION
F-XY FILTER
3D PHASE SHIFT MIGRATION
BANDPASS FILTER
TIME VARIANT SCALING

Fig.6. Sensor's vertical processing flow

Although the signal to noise ratio was much worse than for the P-wave sections, converted wave stacks were greatly enhanced by the velocity-specific, F-K and F-XY filtering. Representative inline and crossline cross sections of the final migrated stacked volumes are shown in figures 7-14.

CONCLUSIONS

Standard vertical processing flows produced very good results. Birefringence analysis showed that shear wave splitting was negligible yielding a single horizontal component stacked volume. Three binning methods showed that asymptotic binning represents a good first guess while DMO binning is the most accurate way of determining P-S wave conversion points. While vertical component's processing was expected to yield good results, radial component's stacks were greatly helped by three shear sonic logs in the area, providing accurate Vp/Vs ratios.

ACKNOWLEDGMENTS

I would like to thank John Boyd of Boyd-Petrosearch and Sue Jones of Kestrel Data for helping me sift through and organize numerous files, sections, films, tapes and floppies that comprise the Blackfoot database.

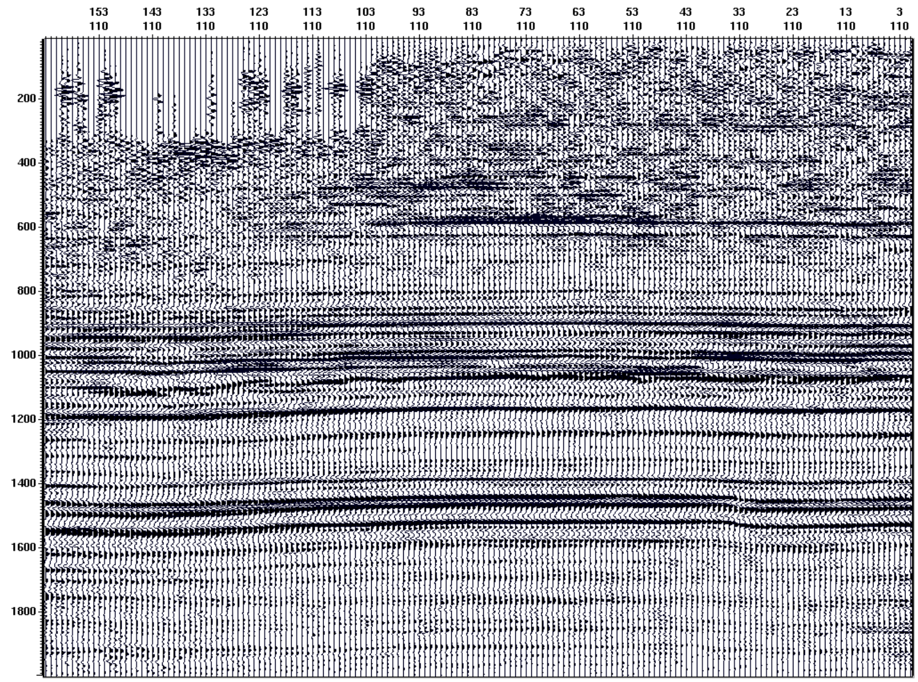

Fig.7. Inline 110 display from Pulsonic's vertical migrated volume

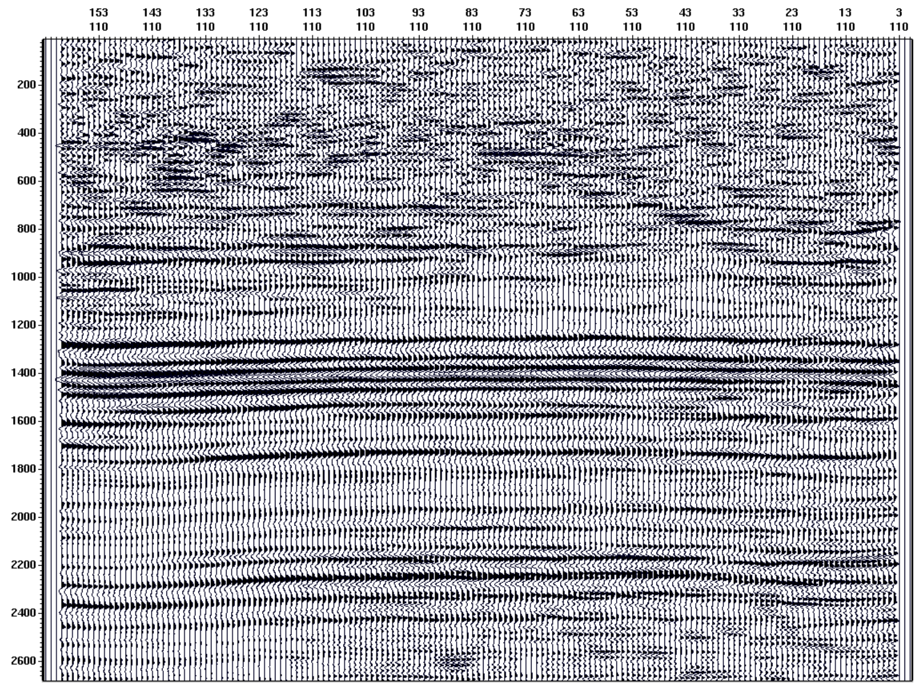

Fig.8. Inline 110 display from Pulsonic's radial migrated volume

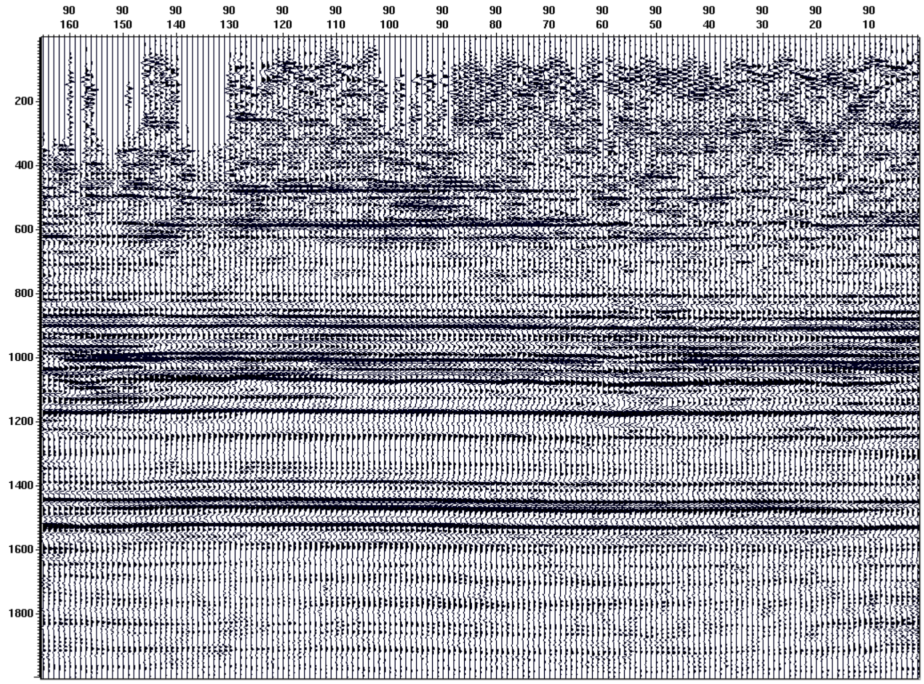

Fig.9. Crossline 90 from Pulsonic's vertical migrated volume

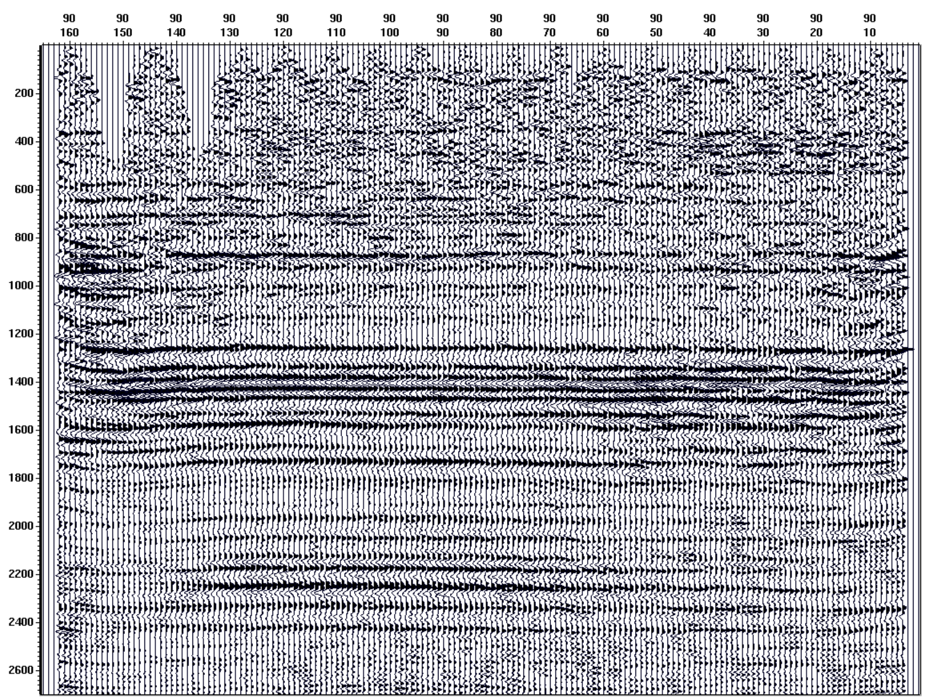

Fig.10. Crossline 90 from Pulsonic's radial migrated volume

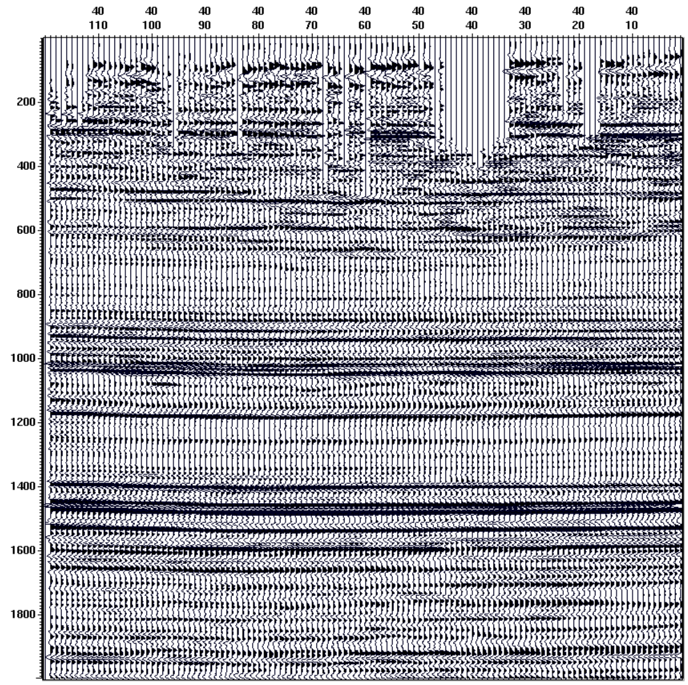

Fig.11. Crossline 40 from Sensor's vertical migrated volume

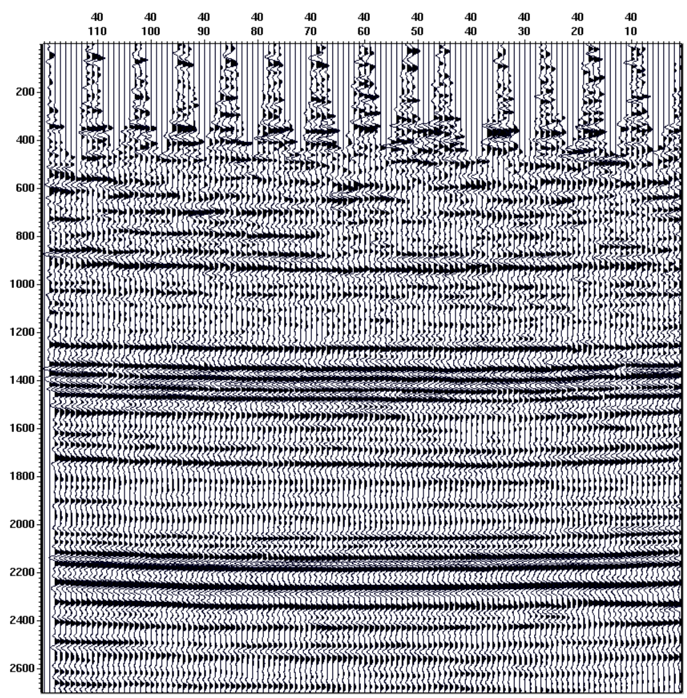

Fig.12. Crossline 40 from Sensor's radial migrated volume

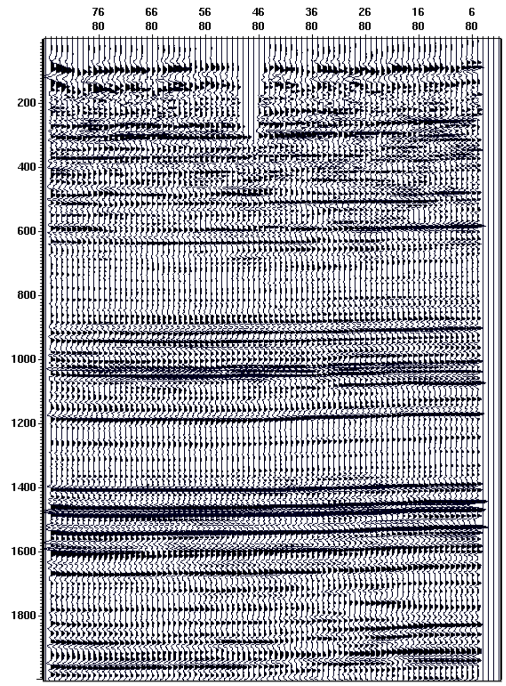

Fig.13. Inline 80 from Sensor's vertical migrated volume

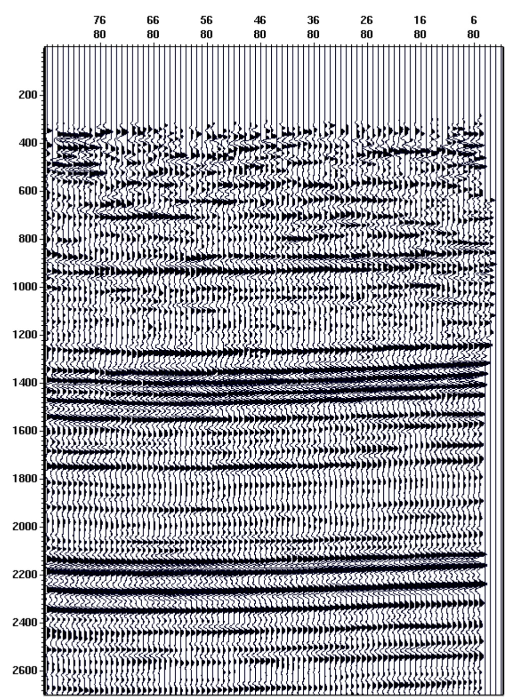

Fig.14. Inline 80 from Sensor's radial migrated volume